Electronic Supplementary Information

Polylactic Acid Based Janus Membrane with Asymmetric Wettability for Directional Moisture Transport and Enhanced UV Protective Capacity

Yingshu Gu, Jing Wu, Miaomiao Hu, Haohong Pi and Rui Wang, Xiuqin Zhang**

Beijing Key Laboratory of Clothing Materials R & D and Assessment, Beijing Engineering Research Center of Textile Nanofiber, School of Materials Design & Engineering, Beijing Institute of Fashion Technology, Beijing 100029, China
E-mail: a.wujing@163.com; clyzxq@bift.edu.cn

S1: SEM images of pristine PLA fabric and TiO_2@PDA-PLA fabric

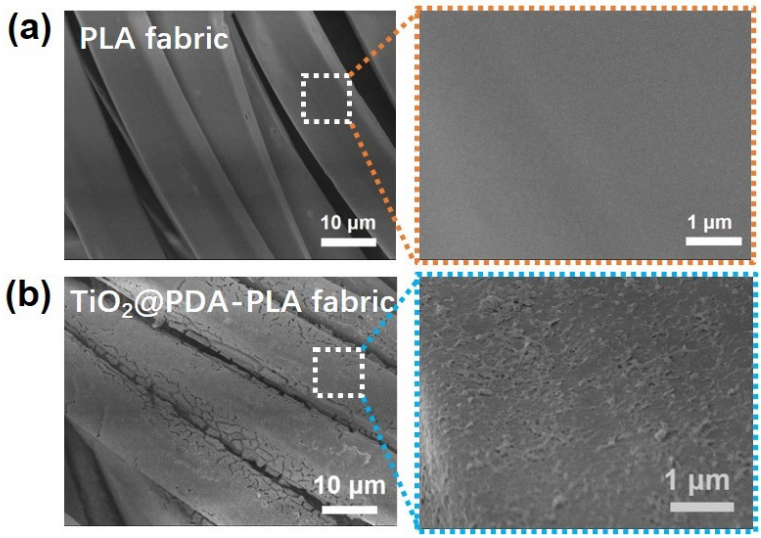

Figure S1: (a) SEM image of pristine PLA fabric (Left) and partial enlarged image (Right). (b) SEM image of TiO_2@PDA-PLA fabric (Left) and partial enlarged image (Right). The average diameter of PLA fabric is about 13.3 μm. After TiO_2 anchoring, the surface of PLA fabric become rough.

S2: Live photos of water droplets dripped on PDA-PLA and TiO_2@PDA-PLA fabrics

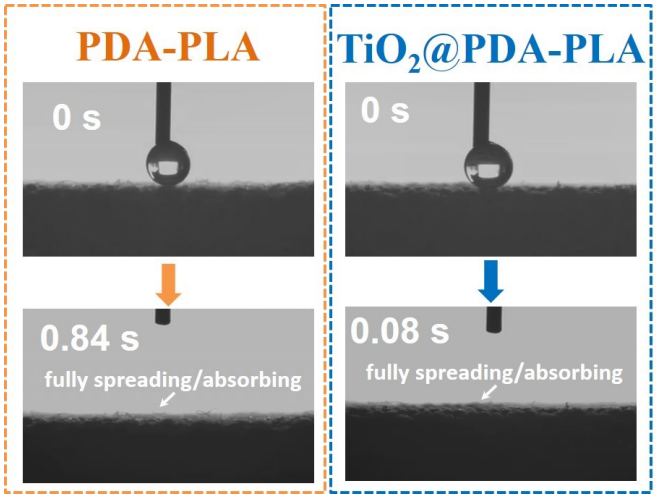

Figure S2. Live photos of water droplets changing on the PDA-PLA and TiO_2@PDA-PLA fabric. In general, both the PDA-PLA and TiO_2@PDA-PLA fabrics shown superhydrophilicity. Water fully spread and adsorb on the surface within 1 s. The difference only exhibited on water spreading time. That is when water droplet was dripped on the PDA-PLA surface, it was fully adsorb in 0.84 s. While, it took very shorter time when spread on TiO_2@PDA-PLA fabric (0.08 s).

.

S3: Analysis of PLA-E fibers

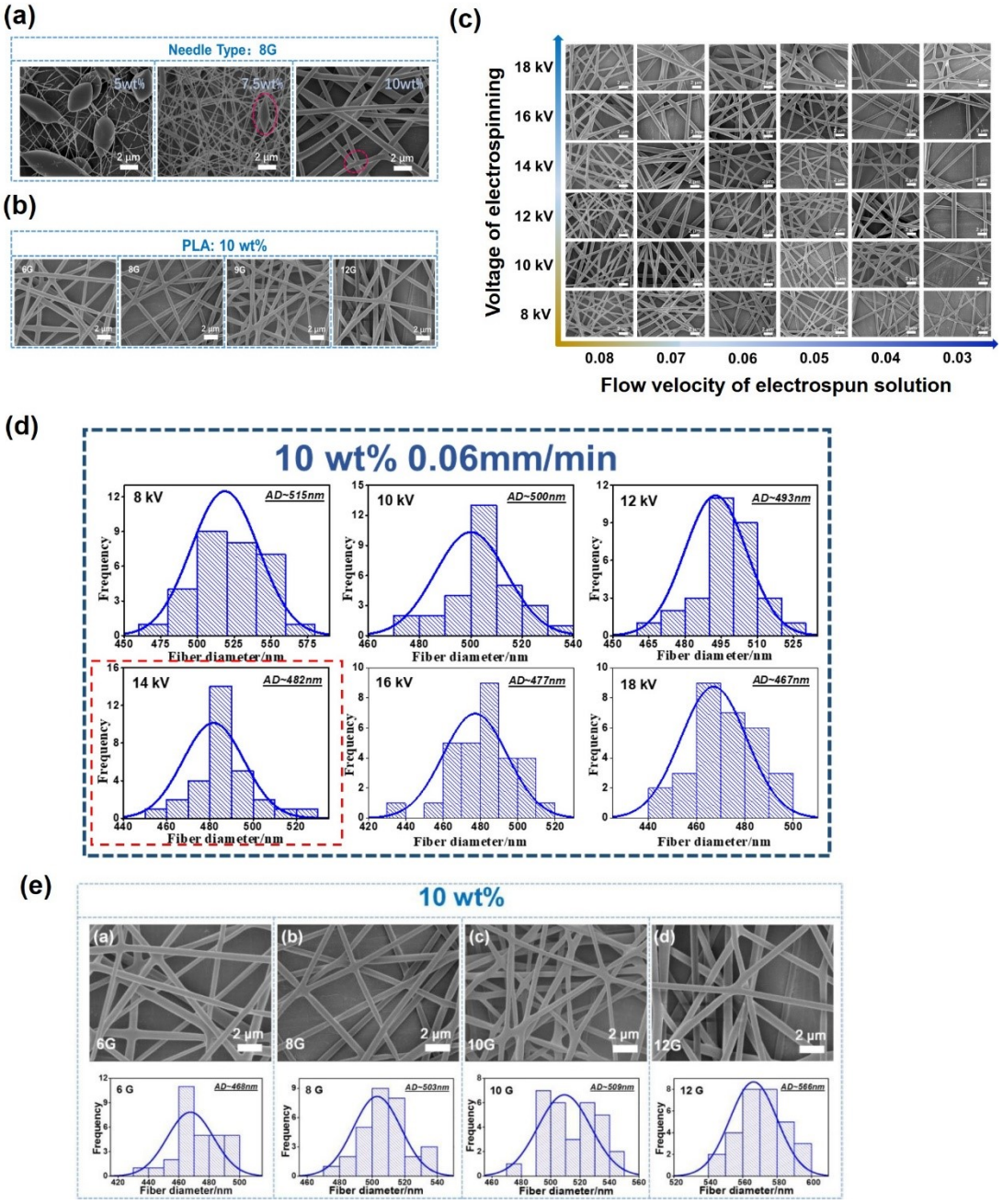

Figure S3. (a) The effects of different concentrations of electrospun solutions on the morphology of PLA nanofibrous films. The concentrations of PLA electrospun solution are 5 wt%, 7.5 wt% and 10 wt%, respectively. The inner diameter of the metal needle nozzle is 0.8mm (named as 8G). (b) The influences of different inner diameters of the electrospun needle nozzles on the morphology of PLA fibrous films. The electrospun needle nozzle with the inner diameter of 0.6 (6G), 0.8 (8G), 1.0 (10G), and 1.2mm

(12G) were equipped during the fabrication process. The concentration of PLA electrospun solution is 10 wt%. (c) The effect of voltage and flow velocity on the morphology of PLA nanofibrous during the electrospinning process. The voltage was set as 8~18 kV, and the flow velocity was controlled to 0.03~0.08 mm/min by the injection pump. (d) Average fiber diameter of PLA fiber prepared with the optical experimental condition that the solution concentration of 10 wt% and flow velocity of 0.06 mm/min. (e) Morphologies of PLA-E membranes fabricated by the PLA concentration of 10 wt% and different electropun nozzle diameter.

S4: EDS analysis of pristine PLA fabric

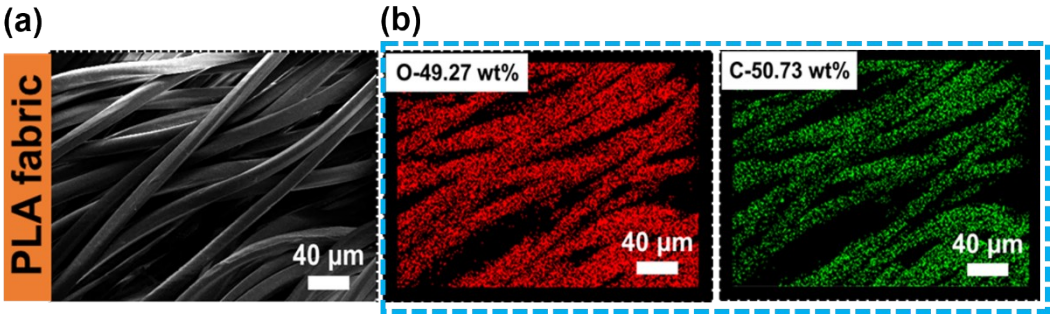

Figure S4. (a) SEM image of pristine PLA fabric. (b) EDS maps of pristine PLA fabric. It can be seen that the content of O and C were 49.27% and 50.73%, respectively.

S5: The relationship between PLA electrospinning time and the Janus membrane

thickness

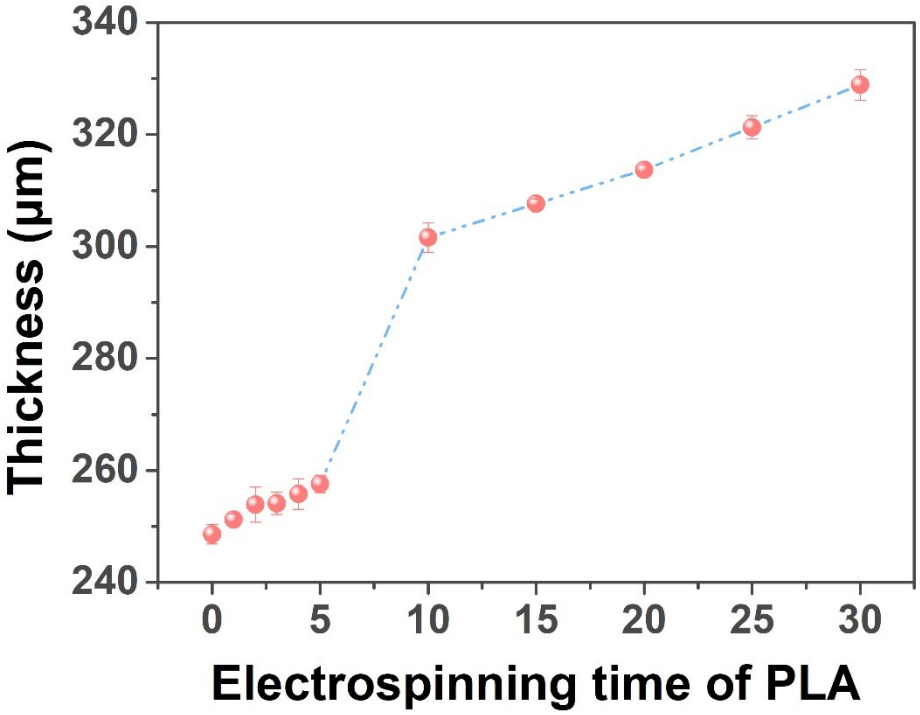

Figure S5. The thickness of Janus membrane vs the electrospinning time of PLA.

S6. Water content of PLA-E(8G)/TiO_2@PDA-PLA and PLA-(12G)/TiO_2@PDA-PLA

Janus membranes.

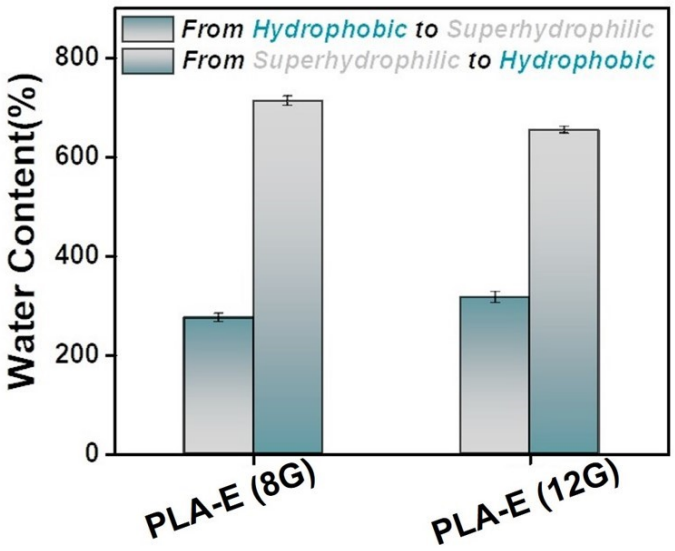

Figure S6. Moisture-management testing (MMT) results of Janus membranes fabricated with different PLA-E average fiber diameters. The average fiber diameters of PLA-E (8G) and PLA-E (12G) are 482 nm and 556 nm, respectively. When water dripped on hydrophobic PLA-E side, the water content of PLA-E(8G)/TiO_2@PDA-PLA was less than that of PLA-E(12G)/TiO_2@PDA-PLA. When water dripped on superhydrophilic TiO_2@PDA-PLA side, PLA-E(8G)/TiO_2@PDA-PLA contained more water than PLA-E(12G)/TiO_2@PDA-PLA, indicating PLA-E(8G)/TiO_2@PDA-PLA with smaller average fiber diameter owns better directional moisture transport capacity.

S7: SEM images of cross-section of Janus membrane fabricated with different PLA-E electrospinning time and the porosities.

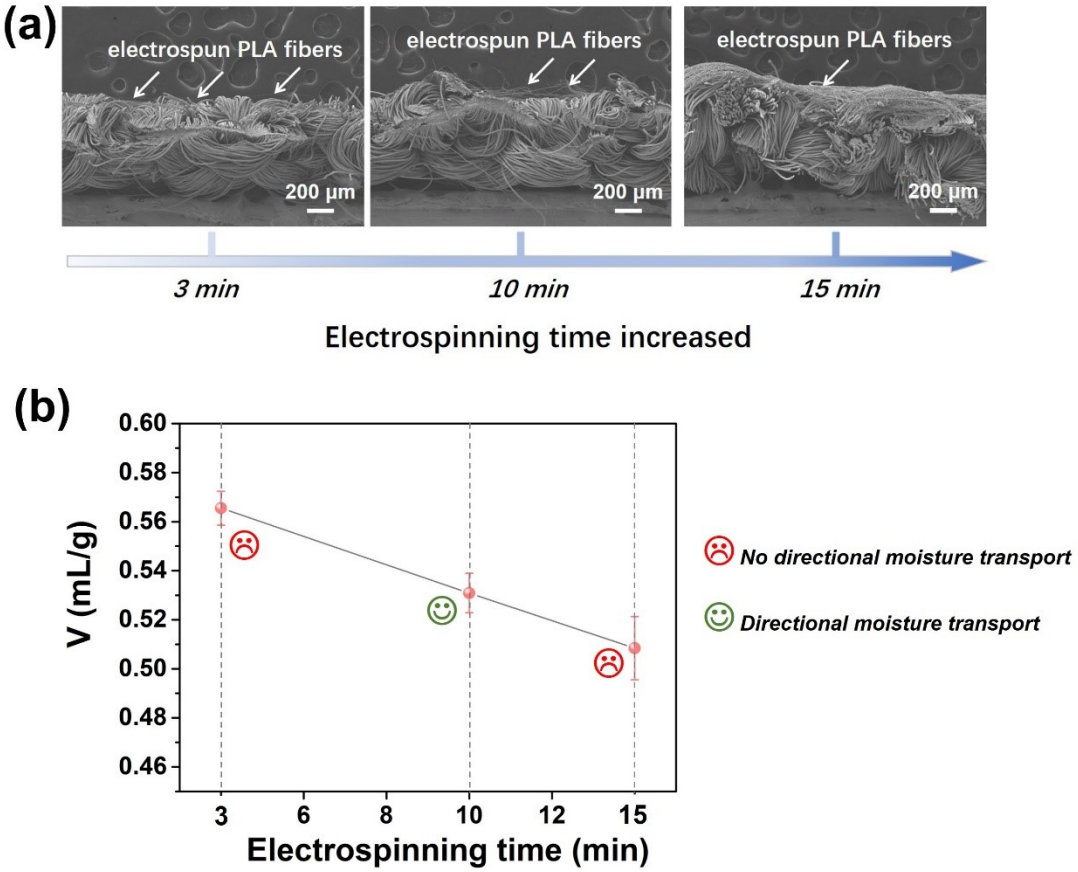

Figure S7. (a) SEM images of cross-section of Janus membrane prepared with different PLA-E electrospinning time, showing morphologies of membrane with different thickness of PLA-E layers. In general, it can be seen that with the increasing of electrospinning time, the thickness of PLA-E layer increased. For the membranes when PLA-E was electropun for 3 mins or 15 mins, the Janus membrane have not shown directional moisture transport capacity. While, when PLA-E electrospun 10 mins, the membrane exhibited directional moisture transport. (b) The corresponding porosity of the above-mentioned samples were measured by pore volume (V). The value V was estimated though uptake of ethyl alcohol to express the porosity. Since ethyl alcohol is nonsolvent for PLA, it can only enter into the pores of the polymer networks. It can be seen that the porosity decreased slightly with the prolonged electrospinning time. [1, 2].

S8: Mechanical properties of these multifunctional membranes

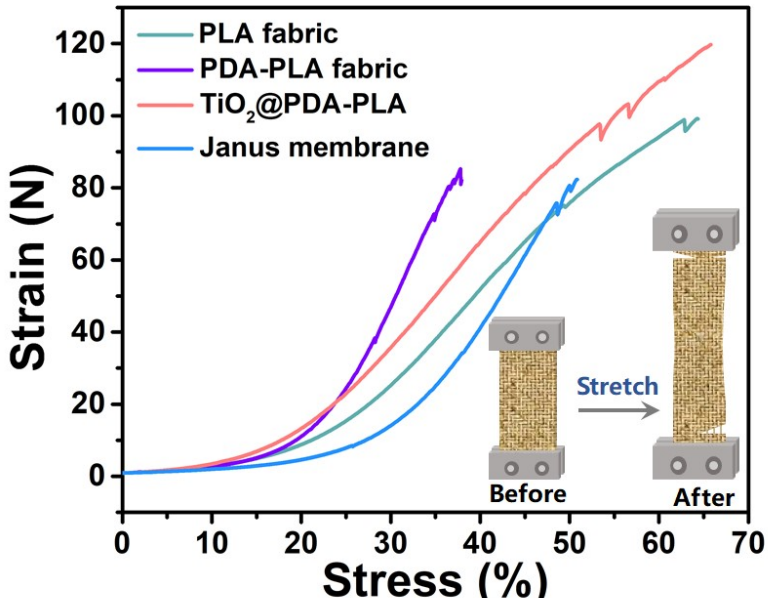

Figure S8. The mechanical properties of PLA fabric, PDA-PLA fabric, TiO_2@PDA-PLA fabric and the PLA-E/TiO_2@PDA-PLA Janus membrane. The tensile strength-elongation at break curves of PLA fabric, PDA-PLA fabric, TiO_2@PDA-PLA fabric and the PLA-E/TiO_2@PDA-PLA Janus membrane were measured The tensile strength-elongation at break curves of PLA fabric, PDA-PLA fabric, TiO_2@PDA-PLA fabric and the PLA-E/TiO2@PDA-PLA Janus membrane were obtained to explore their mechanical properties. Due to the braided structure of the fabric, all samples were not fully stretched to break. Once the fabric was stretched cracking, the testing process was ended. All of the samples exhibited relative higher tensile strength that can need the basic need of clothing. It also can be seen that the Janus membrane shown relatively poor mechanical strength which can be attributed to the two composited layer (electrospun fibrous membrane combined with fabric). When the Janus membrane was stretched, the electrospun fibrous layer break at first, then the fabric layer break under the continuous stretching.

Reference

[1] J. Zheng, A. He, J. Li, J. Xu, C. C. Han, Polymer, 2006, 47,7095-7102.

[2] J. Wu, N. Wang, L. Wang, Y. Zhao, L. Jiang, ACS Appl. Mater. Interfaces, 2021, 4, 3207-3212.